scientific reports

Check for updates

OPEN

The protective effects of propolis against lipopolysaccharide-induced acute liver injury by modulating serum metabolites and gut flora

Zhengxin Liu[1], Zongze Li[1], Yuyang Guo[1], Yajing Li[2]✉ & Hongzhuan Xuan[1]✉

Propolis has significant hepatoprotective effects, but the active components, targets, and mechanisms have not been fully elucidated. Here, we integrated network pharmacology, serum metabolomics, and 16 S rRNA sequencing to disclose the hepatoprotective effects of Chinese propolis (CP) by lipopolysaccharide (LPS)-induced acute liver injury (ALI) in mice. The core active ingredients of CP against ALI, including quercetin, luteolin, and kaempferol, can bind stably to pro-inflammatory factors such as TNF-α, IL-6, IL-1β, and IFN-γ. CP and its active ingredient quercetin obviously alleviated LPS-induced ALI in mice and downregulated the levels of pro-inflammatory genes (*Tnf-α*, *Il-1β*, *Il-6*, *Mcp-1*, *Ifn-γ*, and *Cox-2*) while increasing the protein expression levels of the antioxidant factors Nrf2 and HO-1. Untargeted serum metabolomics analysis indicated that CP and quercetin ameliorated LPS-induced metabolic disorders mainly by modulating the ascorbate and aldarate metabolisms. 16 S rRNA sequencing demonstrated that CP and quercetin modulated the gut microbiota, augmenting the relative abundance of anti-inflammatory bacteria like *Lactobacillus* and *Dubosiella* and diminishing the pro-inflammatory bacteria like *Alistipes*. Spearman correlation analysis revealed that there existed significant correlations among inflammatory factors, gut microbiota, and differential metabolites of serum after propolis pretreatment. Our research indicated that propolis effectively alleviated pathological damage in LPS-induced ALI mice mainly through partially restoring the ecology of gut flora and metabolic disorders to reduce inflammation.

Keywords Chinese propolis, Quercetin, Acute liver injury, Network Pharmacology, Metabolomics, Gut flora

Propolis, a natural bee product collected by honey bees from plant resins, exhibits a wide array of biological activities, such as antioxidant, anti-inflammatory, antitumor, hepatoprotective, and immunomodulatory effects[1]. Thus, propolis has been long used as a health food and medicine for the promotion of human health and the prevention of disease. Current studies have shown that propolis has significant hepatoprotective effects, but the active components, targets, and mechanisms by which propolis exerts hepatoprotective activity have not been fully elucidated.

The liver, an essential organ in humans, performs various functions, including metabolism and detoxification. Liver damage, caused by factors such as bacterial and viral infections, toxic medications or toxins, alcohol addiction, etc., can lead to hepatocyte apoptosis, necrosis, and steatosis[2]. Severe acute liver injury (ALI) may induce hepatic encephalopathy, systemic multi-organ failure, and other complications, posing significant risks to human health[3]. Controlling the onset and progression of liver injury is crucial in liver disease management. However, due to the limited therapeutic options, it is essential to explore effective drugs for treating liver injury.

Numerous studies have established the pivotal roles of oxidative stress and inflammation in the onset of liver disease[4,5]. Oxidative stress and inflammation endure and interact with one another to cause a vicious cycle that exacerbates the development of liver disease, ranging from steatosis to fibrosis, cirrhosis, and hepatocellular cancer[6]. The utilization of antioxidants and anti-inflammatory drugs in liver disease treatment has been extensively studied.

Propolis possesses potent antioxidant and anti-inflammatory properties, and an expanding body of research has demonstrated its hepatoprotective effects through antioxidative and anti-inflammatory mechanisms[7,8]. Turkish propolis significantly reduced aluminum chloride-induced liver toxicity in rats[9]. da Silva et al. (2016)

[1]School of Life Sciences, Liaocheng University, Liaocheng 252059, China. [2]The Department of Biopharmaceutical Technology, Zhejiang Institute of Economics and Trade, Hangzhou 310018, China. ✉email: jjcyly@163.com; hongzhuanxuan@163.com

reported that Brazilian green propolis also mitigated secondary hepatic inflammation induced by Leishmania amazonensis[10]. Additionally, Sefrou propolis demonstrated the ability to alleviate oxidative stress and ameliorate gentamicin-induced liver damage[11]. Therefore, utilizing propolis and its derived compounds to protect and enhance liver health shows promise as a therapeutic approach.

In addition to oxidative stress and inflammation, an increasing number of studies suggest a close association between gut flora and liver disease progression[12]. Research indicates that propolis significantly impacts liver-related diseases by modulating the composition of gut microbiota. In high-fat diet-induced obese mice, propolis alleviated hyperlipidemia and hepatic steatosis by restructuring the intestinal flora to increase the abundance of anti-obesity and anti-inflammatory bacteria while decreasing the abundance of proinflammatory bacteria[13,14]. Brazilian green propolis increases the Bacteroidetes/Firmicutes ratio and abundance of *Butyricicoccus* and *Acetivibrio* in db/db mice and alleviates sarcopenic obesity[15]. However, the influence of propolis on ALI through the restructuring of intestinal flora has not been reported. In addition to altering the composition of gut microbiota that impacts liver disease, the derived components and metabolites produced by these microbiotas are also crucial in regulating the pathological processes associated with liver disease. These components and metabolites are transported to the liver via the portal vein[16]. Various immune cells in the liver respond to pro-inflammatory factors of intestinal origin, such as lipopolysaccharides (LPS), peptidoglycans, and lipoteichoic acid, which may become over-activated and trigger more severe liver injury. On the other hand, short-chain fatty acids, bile acids, tryptophan metabolites, and phenolic metabolites derived from intestinal flora may ameliorate inflammatory responses and oxidative damage in liver tissue[17]. Thus, the composition of gut microbiota and its metabolites are key factors in regulating liver injury.

Network pharmacology, an emerging discipline, utilizes computer-aided databases to construct the "component-target-pathway-disease" network, facilitating the prediction of active ingredients, targets, and signaling pathways of complex natural products against various diseases[18]. Propolis possesses a highly complex chemical composition, with over 800 chemical components identified to date[19]. Given the complexity of propolis's chemical components, network pharmacology offers a method for identifying the active components and elucidating the mechanisms underlying propolis's hepatoprotective effects.

Although propolis has shown efficacy in alleviating liver injury, there remains limited understanding regarding its active constituents, targets, and molecular mechanisms for liver injury and its effect on the gut-liver axis. Here, for the first time, a widely targeted metabolomic approach was employed to comprehensively elucidate the chemical composition of propolis. Subsequently, the active components, targets, and signaling pathways of propolis for improving ALI were confirmed through network pharmacology and molecular docking. Furthermore, serum metabolomics and gut flora analysis were employed to assess the effects and mechanisms of propolis and its active ingredients in ALI mice. The present study will provide the theoretical and experimental groundwork for propolis as a health food and medicine in the mitigating of liver injury.

Results

Network pharmacological analyses

Construction of the PPI network for common targets of CP and ALI as well as hub gene screening

A total of 2083 components were identified in CP through UPLC-MS/MS analysis, with flavonoids having the most abundance (Fig. 1a). Based on the 2083 components, 119 components met the screening criteria (Table S1), and a total of 664 gene targets were acquired. And 2479 gene targets for ALI were obtained by merging and deduplication. The Venn diagram (Fig. 1b) reveals 342 common targets between the active ingredients of CP and ALI. These common targets produced a PPI network diagram (Fig. 1c), from which the top 30 hub genes were selected by calculating the degree values (Table S2) and creating a visual network diagram. These hub genes are expected to play a key role in ALI treatment with CP. Notably, inflammation-related genes including TNF-α, IL-6, IL-1β, and IFN-γ were identified, suggesting that CP and its active ingredients may target inflammatory factors against ALI.

GO and KEGG analyses of the common targets of CP and ALI The top 10 of the BP, CC, and MF involved in ALI treatment with CP are shown in Fig. 1d. BP was enriched in the inflammatory response, response to lipopolysaccharide, and cellular response to lipopolysaccharide. CC predominantly consisted of the cell surface, membrane raft, and cytosol. MF included enzyme binding, protein binding, etc. Additionally, signaling pathways associated with inflammation such as PI3 K-Akt, TNF, and IL-17 were enriched, suggesting CP and its key components primarily targeted inflammatory signaling pathways against ALI (Fig. 1e).

The core component screening of CP in the treatment of ALI with CP A "CP-key components-common targets-major pathways-ALI" network was constructed (Fig. 2a). The 119 active components of CP were ranked based on their degree values, revealing quercetin, luteolin, and kaempferol as the top three core components (Table S3). Besides these, isorhamnetin, naringenin, galangin, formononetin, kaempferide, dihydrokaempferol, acacetin, taxifolin, diosmetin, pinocembrin, chrysin, and genistein were also identified as core components of CP against ALI.

Results of molecular docking of CP's core components and inflammatory genes

Based on the affinity heatmap depicted in Fig. 2b, the average affinity value of the top three core components of CP with inflammatory gene targets was − 6.85 kcal/mol. Furthermore, all three core components of CP exhibited affinity values to inflammatory gene targets of less than − 5 kcal/mol, suggesting their high affinity and stability. The primary binding mechanism of the top three core components of CP to inflammatory gene targets involves hydrogen bonding and hydrophobic interactions (Fig. 2c-n). Besides, quercetin also interacts with TNF through π-Stacking (P-type) and π-Stacking (T-type) interactions, while interacting with IFN-γ through π-Cation

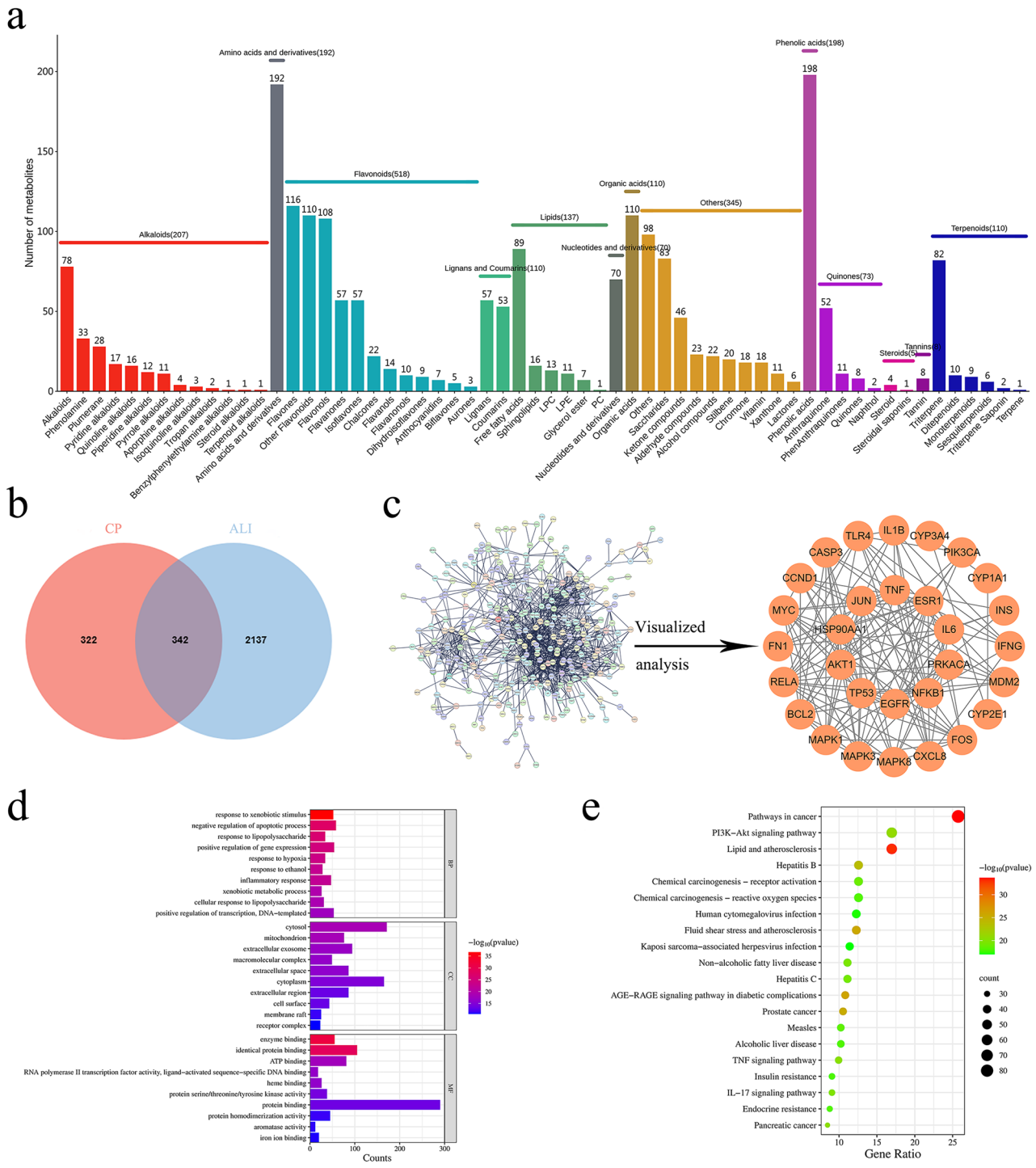

Fig. 1. Construction of the PPI network and GO and KEGG analyses of the common targets. (**a**) UPLC-MS/MS analysis on CP. (**b**) The Venn diagram of the overlapping targets of the active components between CP and ALI. The red circle represents the target of the active components of CP, and the blue circle signifies ALI's targets. (**c**) The PPI network and the visualization of the top 30 hub genes of CP in the treatment of ALI. The orange nodes represent the potential therapeutic targets of the active components of CP against ALI. (**d**) GO enrichment analysis bar with color gradients. (**e**) Bubble plots for KEGG pathway enrichment analysis.

interactions. Similarly, luteolin and kaempferol exhibit π-Stacking and π-Cation interactions with TNF and IFN-γ, respectively.

To further assess the efficacy of CP and its primary components against ALI, we chose the top core ingredient, quercetin, for the following experiment.

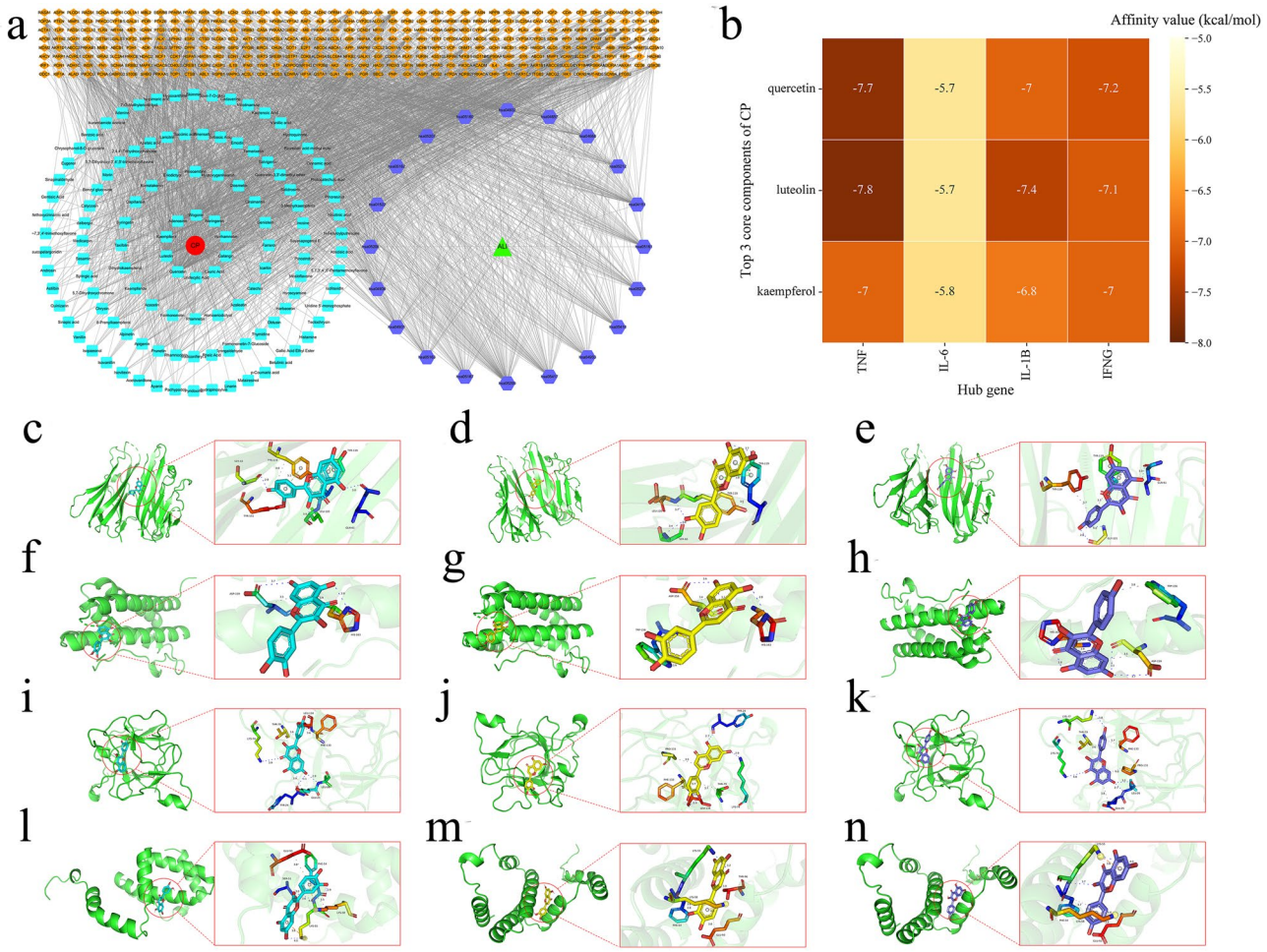

Fig. 2. Screening of the top three core components and results of molecular docking. (**a**) The network of CP-key components-common targets-major pathways-ALI. The red circle is CP, the blue rectangles are the 119 key components, the orange rhombuses are the 342 key targets, the purple hexagons are the KEGG numbers of the 20 major pathways, and the green triangle is ALI. (**b**) Heatmap of the affinity value. The darker color represents lower binding energy for the core component and hub gene, signifying a more stable binding conformation. (**c**-**n**) The visualization of molecular docking. Blue molecules for quercetin, yellow molecules for luteolin, and purple molecules for kaempferol. Hydrogen bonds are depicted by blue dashed lines, hydrophobic interactions by grey dashed lines, π-stacking (P-type) interactions by light-green dashed lines, π-stacking (T-type) interactions by dark-green dashed lines, and π-cation interactions by orange dashed lines. (**c**) TNF-Quercetin. (**d**) TNF-Luteolin. (**e**) TNF-Kaempferol. (**f**) IL-6-Quercetin. (**g**) IL-6-Luteolin. (**h**) IL-6-Kaempferol. (**i**) IL-1β-Quercetin. (**j**) IL-1β-Luteolin. (**k**) IL-1β-Kaempferol. (**l**) IFN-γ-Quercetin. (**m**) IFN-γ-Luteolin. (**n**) IFN-γ-Kaempferol.

CP and quercetin treatments alleviated liver injury in ALI mice

Figure 3a illustrated the ALI model and the treatment. Except for the normal group, all mice were injected with LPS in the tail vein 24 h after the last dose and fasted for 12 h after the injection to establish an ALI mouse model. There was no significant change in the body weight of mice during gavage (Fig. 3b). Furthermore, as shown in Fig. 3c and d, the ratio of spleen or kidney weight to body weight significantly increased in the LPS-treated group, while CP restored both indices. Quercetin also reduced the spleen index but did not significantly alter the kidney index compared to the LPS group. These data reflect the non-toxicity of CP and quercetin treatment and the toxicological effects of LPS.

H&E staining revealed that LPS stimulation led to eosinophilic degeneration and atrophy of hepatocytes, deep eosin staining in the cytoplasm, reduced nuclear size, structural disorganization of liver tissue, and localized infiltration of inflammatory cells (Fig. 3e). Conversely, hepatic necrosis was greatly reduced with minimal histological alterations after CP and quercetin treatment, suggesting CP and quercetin had a protective effect on ALI mice. Moreover, we measured the activities of alanine aminotransferase (ALT) and aspartate aminotransferase (AST) in liver tissue. As shown in Figure S1, LPS treatment led to a significant increase in ALT and AST activities, indicating liver injury. However, treatment with CP and quercetin effectively reduced these enzyme activities, confirming their protective effects against ALI.

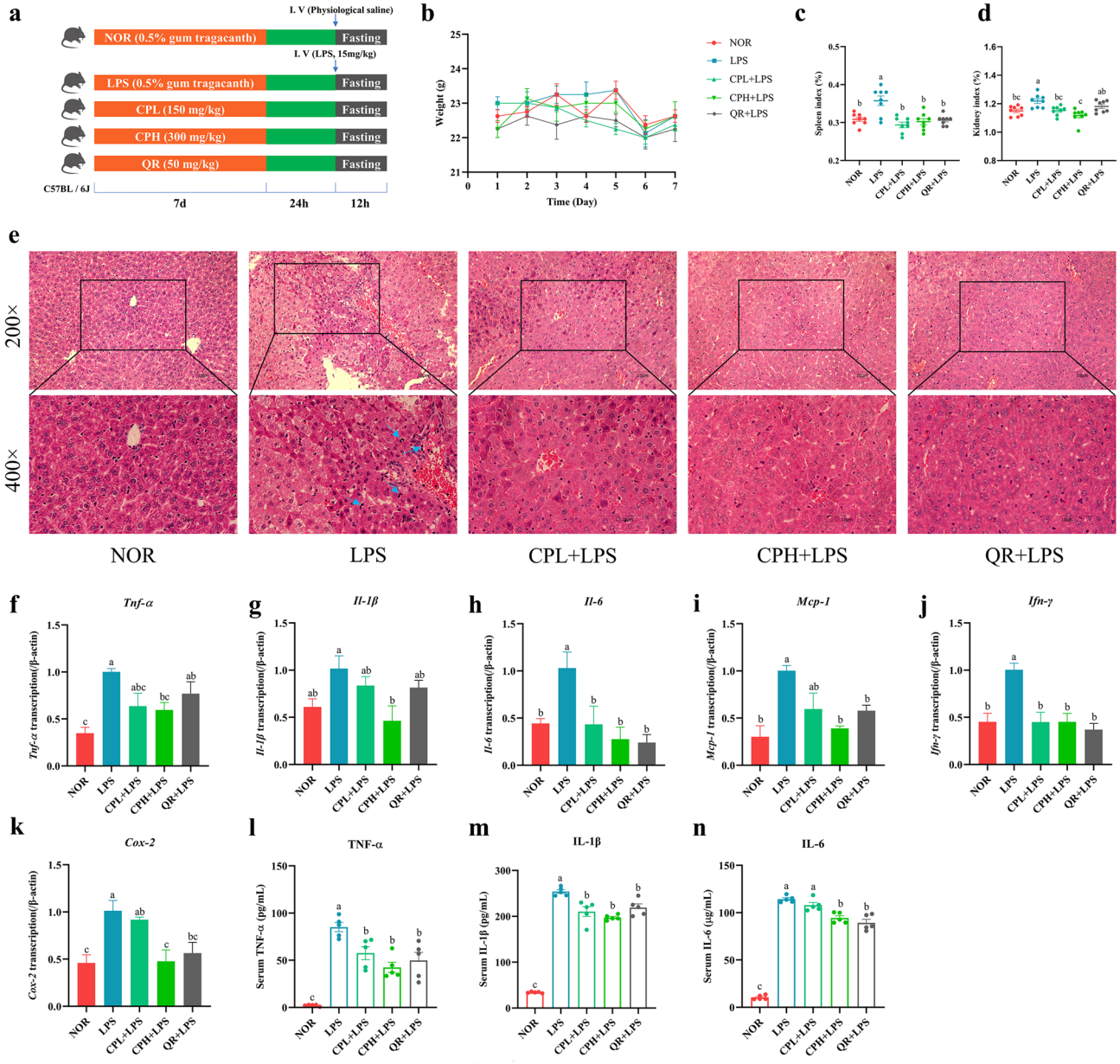

Fig. 3. CP and quercetin treatments alleviated LPS-induced ALI in mice. (**a**) Establishment of a mouse model with LPS-induced ALI. (**b**) Body weight changes of mice in various groups during gavage. (**c**) Spleen weight-to-body weight ratio. (**d**) Kidney weight-to-body weight ratio. (**e**) H&E staining of mouse liver tissue. Blue arrows point to eosinophils. (**f**-**k**) *Tnf-α*, *Il-1β*, *Il-6*, *Mcp-1*, *Ifn-γ*, and *Cox-2* mRNA expression levels in liver tissues. Serum (**l**) TNF-α, (**m**) IL-1β, and (**n**) IL-6 levels were determined by ELISA. All data are expressed as mean ± SEM, $n = 3$ (**f**-**k**), 5 (**l**-**n**), or 8 (**b**-**d**) per group. Different superscript letters denoting significant differences ($P < 0.05$). (NOR: normal group, LPS: model group, CPL + LPS: low-dose propolis treated group, CPH + LPS: high-dose propolis treated group, QR + LPS: quercetin treated group).

CP and quercetin treatments reduced inflammatory factor levels and increased antioxidant factor levels in ALI mice

LPS stimulation upregulated mRNA expression levels of T*nf-α*, *Il-1β*, *Il-6*, *Mcp-1*, *Ifn-γ*, and *Cox-2* in mouse liver tissues compared to the normal group, whereas pretreatment with CP and quercetin decreased these gene expressions (Fig. 3f-k). Furthermore, the results from the ELISA assay of the serum also indicated that CP and quercetin pretreatment obviously suppressed the levels of TNF-α, IL-1β, and IL-6 compared with the LPS group (Fig. 3l-n). These results indicated that CP and quercetin had significant anti-inflammatory properties against ALI, and CP with a high dose exhibited more significant effects in reducing the levels of pro-inflammatory factors.

Western blot results (Figure S2) show that LPS stimulation significantly elevated IL-1β expression, while CP and quercetin treatment reduced it. Furthermore, both treatments upregulated the levels of the antioxidant factors Nrf2 and HO-1 compared to the LPS group, suggesting CP and quercetin enhanced antioxidant capacity and anti-inflammatory effects in ALI mice.

CP and quercetin treatment modulated the serum metabolites in ALI mice

Untargeted metabolomics was performed to analyze serum metabolite changes. The PCA score plot (Fig. 4a, b) illustrated distinct distributions of metabolic profiles among the five groups in both negative and positive ion modes, suggesting significant impacts of CP and quercetin pretreatment on serum metabolites in ALI mice. The OPLS-DA model also demonstrated distinct separation among different groups (Fig. 4c, d). After 200 permutation tests (Fig. 4e, f), the intersection of the Q^2 regression line with the vertical axis was below zero, affirming the model's validity and absence of overfitting[20].

The cluster heatmaps revealed the differences in serum metabolites among different groups (Fig. 4g, h). Volcano plots were constructed to identify differential metabolites and the disparities between the normal and LPS groups (Fig. 4i, j), the CPL and LPS groups (Fig. 4k, l), the CPH and LPS groups (Fig. 4m, n), and the

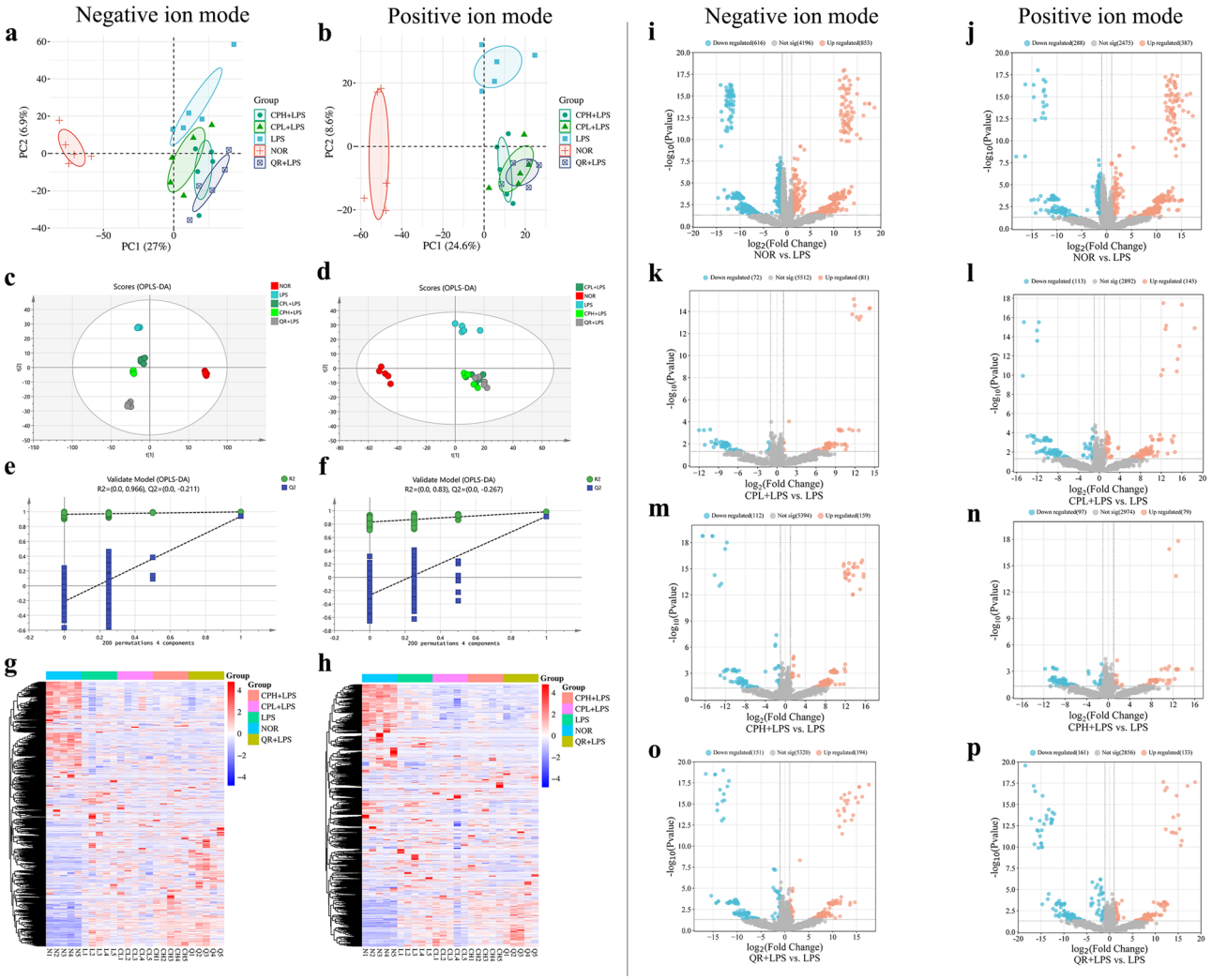

Fig. 4. Modulation of CP and quercetin treatment on serum metabolism in mice with LPS-induced ALI. PCA score plots in negative (**a**) and positive (**b**) ion modes. OPLS-DA score plot in negative (**c**) and positive (**d**) ion modes. Permutation analysis of the corresponding OPLS-DA models in both negative (**e**) and positive (**f**) ion modes. R^2 represents the explained variance, while Q^2 indicates the predictive capability of the model. Cluster heatmap analysis of serum metabolites in negative (**g**) and positive (**h**) ion modes. Volcano plots depict serum metabolites of the normal and LPS groups in both negative (**i**) and positive (**j**) ion modes, the CPL and LPS groups in negative (**k**) and positive (**l**) ion modes, the CPH and LPS groups in negative (**m**) and positive (**n**) ion modes, and the quercetin and LPS groups in negative (**o**) and positive (**p**) ion modes. Blue for metabolites downregulated, red for metabolites upregulated. (NOR, N: normal group, LPS, L: model group, CPL + LPS, CL: low-dose propolis treated group, CPH + LPS, CH: high-dose propolis treated group, QR + LPS, Q: quercetin treated group).

quercetin and LPS groups (Fig. 4o, p). In the negative ion mode, the LPS group exhibited 616 down-regulated and 853 up-regulated metabolites compared to the normal group. Similarly, in the positive ion mode, the LPS group showed 288 down-regulated and 387 up-regulated metabolites compared to the normal group. In contrast, both propolis and quercetin decreased the number of down-regulated and up-regulated metabolites compared with the LPS group, respectively, implying that propolis and quercetin pretreatment reversed part of the serum metabolite changes caused by LPS stimulation in ALI mice.

Effect of CP and quercetin treatment on serum metabolic pathways in ALI mice

KEGG metabolic pathway analysis revealed that the top four pathways were pyrimidine metabolism, pentose and glucuronate interconversions, vitamin B6 metabolism, and ascorbate and aldarate metabolism in negative ion mode (Fig. 5a). Furthermore, the metabolic pathways, including glycerophospholipid metabolism, caffeine metabolism, lysine degradation, and sphingolipid metabolism, were the top four pathways in positive ion mode (Fig. 5b).

Notably, the ascorbate and aldarate metabolism was enriched in the negative ion mode. Previous studies have demonstrated that ascorbate possesses potent antioxidant and anti-inflammatory properties[21]. As shown in Fig. 5c, three metabolites exhibited differential expression among the groups: β-D-glucuronoside, glucuronate, and L-gluconate. The peak heights of these three differential metabolites are presented in Figs. 5d-f. LPS stimulation significantly reduced their levels in mouse serum compared to the normal group. Conversely, propolis and quercetin pretreatment reversed this trend compared to the LPS group. These findings suggested

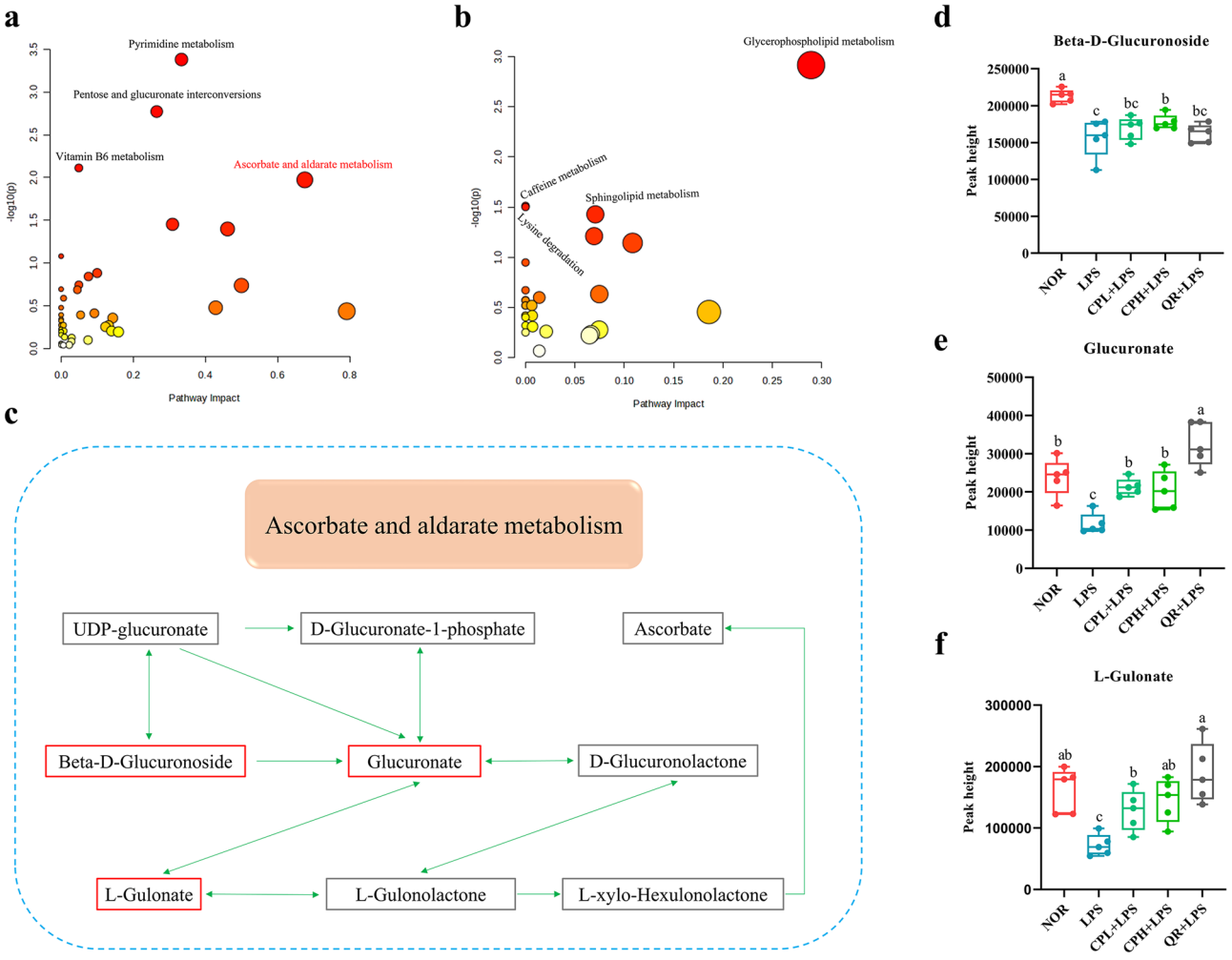

Fig. 5. Effect of CP and quercetin treatment on serum metabolic pathways in mice with LPS-induced ALI. KEGG metabolic pathway enrichment analysis of serum differential metabolites for groups in negative (**a**) and positive (**b**) ion mode. Each circle's size and color were determined by the pathway impact value and *p*-value, respectively. (**c**) Effect of CP and quercetin treatment on ascorbate and aldarate metabolism in ALI mice. Comparison of (**d**) β-D-glucuronoside, (**e**) glucuronate, and (**f**) L-gulonate for different groups in ascorbate and aldarate metabolism. Data for (**d**-**f**) were expressed as mean ± SEM, $n = 5$ per group. Different superscript letters denoting significant differences ($P < 0.05$). (NOR: normal group, LPS: model group, CPL + LPS: low-dose propolis treated group, CPH + LPS: high-dose propolis treated group, QR + LPS: quercetin treated group).

that CP and quercetin may exert anti-inflammatory effects by increasing the levels of β-D-glucuronoside, glucuronate, and L-gluconate to stimulate ascorbate production, thereby enhancing antioxidant capacity and alleviating ALI in mice.

CP and quercetin modulated the gut microbiota in ALI mice

The indices of Ace, Chao, and Sobs are used to reveal community richness, while the indices of Shannon, Simpson, and Invsimpson represent community diversity in the Alpha diversity analysis. LPS stimulation increased community richness and diversity, whereas pretreatment with CP and quercetin reduced this trend, suggesting that CP and quercetin can restore community diversity to normal levels (Fig. 6a-f).

PCoA and NMDS analyses indicated that LPS, CP, and quercetin treatment affected the structure and composition of the gut microbiota in mice (Fig. 6g-j). Notably, an overlap was observed among the quercetin-treated, normal, and LPS groups at the genus level (Fig. 6h, j), indicating quercetin's role in recovering the composition and structure of the mouse gut microbiota from an inflammatory to a normal state. To determine whether the differences in mice's gut microbiota among groups were significant, we used PLS-DA analysis, which revealed a notable difference at the OTU and genus levels (Fig. 6k, l).

CP and quercetin changed the gut microbiota at several taxonomic levels in ALI mice

To investigate the effects of CP and quercetin on the gut microbiota of ALI mice at different taxonomic levels, we generated cluster histograms (Fig. 7a-c) and the changes in major gut microbiota (Fig. 7d-f and Figure S3), as well as the ratio of Firmicutes and Bacteroidetes (F/B ratio, Fig. 7g).

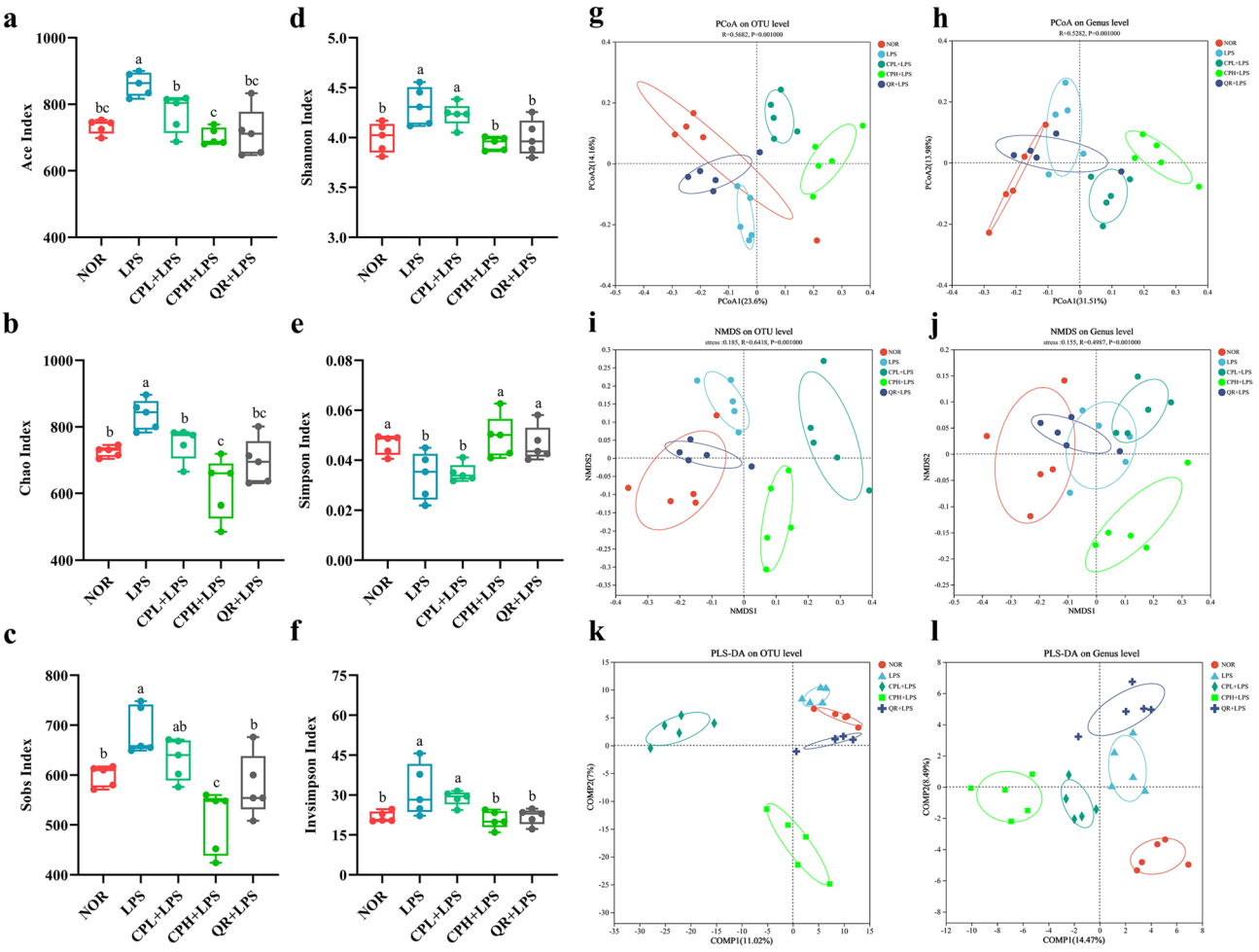

Fig. 6. Effects of CP and quercetin on the diversity of gut microbiota in ALI mice ($n = 5$). The alpha diversity analysis of the gut microbiota in cecal contents, including (**a**) Ace, (**b**) Chao, (**c**) Sobs, (**d**) Shannon, (**e**) Simpson, and (**f**) Insimpson index changes in different groups. PCoA plot on (**g**) OTU level and (**h**) genus level. NMDS plot on (**i**) OTU level and (**J**) genus level. PLS-DA plot on (**k**) OTU level and (**l**) genus level. Data for (**a**-**f**) are expressed as mean ± SEM. Different superscript letters denoting significant differences ($P < 0.05$). (NOR: normal group, LPS: model group, CPL + LPS: low-dose propolis treated group, CPH + LPS: high-dose propolis treated group, QR + LPS: quercetin treated group).

Fig. 7. Relative abundance and differential analysis of gut microbiota in groups. Relative abundances of the gut microbiota at the (**a**) phylum, (**b**) family, and (**c**) genus level. (**d**-**f**) The two most abundant phyla, the three most abundant families, and the four most abundant genera were analyzed separately. (**g**) Ratio of relative abundance of Firmicutes and Bacteroidetes (F/B). (**h**) The top 8 differential gut microbiota at the genus level ($^{*}P < 0.05$, Kruskal-Wallis sum-rank test). (**i**, **j**) LEfSe analysis revealed gut microbiota biomarkers in groups, with LDA > 3. Data for (D-G) are expressed as mean ± SEM, $n = 5$ per group. Different superscript letters denoting significant differences ($P < 0.05$). (NOR: normal group, LPS: model group, CPL + LPS: low-dose propolis treated group, CPH + LPS: high-dose propolis treated group, QR + LPS: quercetin treated group).

Firmicutes and Bacteroidetes were the predominant phyla at the phylum level (Fig. 7a, d). LPS stimulation reduced the relative abundance of the Firmicutes while increasing Bacteroidetes compared to the normal group. Conversely, CP pretreatment reversed this trend compared to the LPS group. These changes led to a convergence in the structure of the gut microbiota between the CP and normal groups. Pretreatment with quercetin also significantly enhanced the relative abundance of the Firmicutes compared to the LPS group but had no significant effect on the Bacteroidetes. Additionally, as illustrated in Fig. 7g, LPS stimulation decreased the F/B ratio, but CP and quercetin pretreatment showed no change compared to the LPS group.

LPS stimulation led to an increase in the relative abundance of Muribaculaceae at the family level (Fig. 7b, e), while decreasing Norank_o_Clostridia_UCG-014. However, high-dose propolis pretreatment restructured the

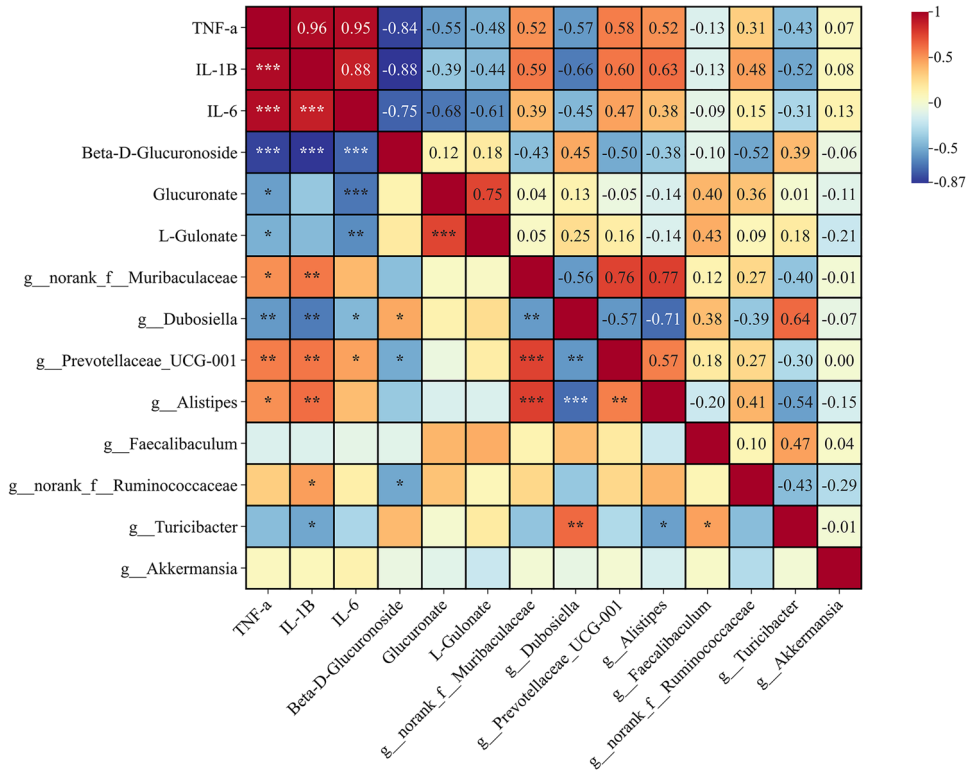

Fig. 8. Spearman correlation analysis of inflammation-related cytokines, differential metabolites of ascorbate and aldarate metabolism, and the top 8 differential gut microbiota. In the visualization, red signifies positive correlations, while blue indicates negative correlations. The intensity of the color reflects the strength of the correlation, with numerical values representing Spearman correlation coefficients.

gut microbiota by reducing the relative abundance of Muribaculaceae compared to the LPS group. These changes made the gut microbiota structure in the CP-treated groups more akin to that of the normal group.

At the genus level (Fig. 7c, f), LPS stimulation increased the relative abundance of *norank_f_Muribaculaceae*, while reducing *norank_f__norank_o___Clostridia_UCG-014* and *Lactobacillus*. Compared to the LPS group, CP and quercetin pretreatment reversed the relative abundance of *Lactobacillus* and *Candidatus_Saccharimonas*, resulting in a colony structure resembling that of the normal group. The KW sum-rank test ($p < 0.05$) was employed to compare differences between groups at the genus level and the top 8 differential gut microbiota among the five groups, with the most difference in mean relative abundance being for *norank__f__Muribaculaceae* (Fig. 7h). LPS stimulation increased the relative abundance of *Alistipes*, while decreasing *Dubosiella* when compared to the normal group, and CP and quercetin reversed these species.

A total of 53 significant discriminatory features were identified across phylum ($n = 4$), class ($n = 5$), order ($n = 5$), family ($n = 14$), and genus ($n = 25$) levels, as confirmed by the LEfSe (LDA > 3) difference analysis results (Fig. 7i, j). Firmicutes were predominantly enriched in the normal and quercetin groups, whereas Bacteroidota showed significant enrichment in the LPS group. Additionally, Verrucomicrobiota and Proteobacteria were primarily concentrated in the CP group.

Correlation analysis among inflammatory factors, differential metabolites, and gut microbiota in ALI mice

To investigate the correlations among inflammatory factors, differential metabolites, and gut microbiota in ALI mice, we performed Spearman correlation analysis. Three inflammatory factors, including TNF-α, IL-1β, and IL-6, three differentially expressed metabolites of ascorbate and aldarate metabolism, and the top 8 differential genera were integrated into the network (Fig. 8). Four of the eight gut genera were significantly correlated with TNF-α, six with IL-1β, and two with IL-6, suggesting that the gut microbiota may influence the levels of inflammation-related cytokines in ALI mice. In addition, β-D-glucuronoside exhibited significantly positive or negative correlations with the gut microbiota.

Discussion

Propolis, a natural product, has been demonstrated to be efficacious in treating liver injury. Here, we revealed the active ingredients, targets, and signal pathway of propolis against ALI via network pharmacology, and an in vivo study demonstrated that propolis and its active ingredients, quercetin, modulated gut microbiota and ameliorated metabolic abnormalities to inhibit the development of inflammation.

The main active components of propolis against ALI are mainly flavonoids and phenolic acids, according to network pharmacology prediction, and the top three active ingredients are quercetin, luteolin, and kaempferol. Studies have indicated that these flavonoids have significant activities against liver damage[22–24]. And the biological process of the active ingredients against ALI involves inflammatory response and response to lipopolysaccharide, suggesting that propolis and its active components directly target lipopolysaccharide-induced liver injury. Furthermore, the hub gene associated with CP against ALI was linked to inflammatory factors like TNF-α, IL-6, IL-1β, and IFN-γ, suggesting that the core components of CP may exert anti-inflammatory activities by decreasing the levels of pro-inflammatory factors. Molecular docking results further demonstrated the interaction between the core components and inflammatory genes. Our study's results are in line with prior research, highlighting the hepatoprotective effects of propolis and quercetin, attributed to their ability to decrease inflammatory factor levels[25,26].

Organ mass is the most sensitive indicator in certain toxicity tests, particularly the spleen and kidney indices, which are crucial for assessing drug dose toxicity[27,28]. We demonstrated that doses of CP and quercetin were safe for mice and did not produce toxicological effects, as indicated by the measurements of body weight, spleen indices, and kidney indices. This result rules out any potential interference from CP and quercetin during LPS-induced ALI. When liver tissue is damaged, it results in structural disorders and infiltration of inflammatory cells[29]. Studies have shown that eosinophils are recruited to the liver during ALI to play an immunomodulatory role[30]. In our study, LPS stimulation resulted in structural disorganization of liver tissue with eosinophilic infiltration, suggesting that LPS-induced liver injury occurred. In contrast, treatment with CP and quercetin led to a reduction in the necrotic area of liver tissue and a significant decrease in eosinophil levels, preliminary indicating that CP and quercetin inhibited the inflammatory response. Additionally, CP and quercetin significantly reduced the levels of inflammatory factors in both liver tissue and serum, further supporting their anti-inflammatory efficacy.

Metabolomics is commonly used to understand physiological processes related to disease progression and to search for new diagnostic or prognostic biomarkers of disease in various organisms[31]. In this study, we conducted an untargeted metabolic analysis of mouse serum and performed a metabolic pathway enrichment analysis of the differential metabolites. Research has demonstrated that uridine inhibits fatty liver by regulating hepatic protein acetylation, indicating a close relationship between uridine homeostasis, pyrimidine metabolism, and hepatic lipid metabolism[32]. In the liver, pentose can contribute to the detoxification process by converting to glucuronic acid, which can also revert to pentose for cellular metabolism under certain conditions. This interconversion is significant in the treatment of Yang Huang syndrome[33]. Vitamin B6 is a water-soluble vitamin known for its anti-inflammatory and antioxidant effects in the liver of a rat model of polymicrobial sepsis[34]. In our study, we found that pyrimidine metabolism, pentose and glucuronate interconversions, and vitamin B6 metabolism were significantly enriched. Another study on serum metabolomics in mice with concanavalin A-induced liver injury demonstrated that glycerophospholipid metabolism plays a crucial role in the early stages of liver injury[35]. Additionally, caffeine metabolism, lysine degradation, and sphingolipid metabolism have been shown to significantly influence liver immunomodulatory processes[36–38]. This suggests that these metabolic pathways play an important role in the regulation of liver injury.

Importantly, we found ascorbate and aldarate metabolism. Ascorbate, also known as vitamin C, exhibits potent antioxidant, anti-inflammatory, anti-fibrotic, and anti-angiogenic effects[39]. Xu et al. (2022) demonstrated the significant inhibitory effect of ascorbic acid on oxidative stress, which helped to synergize with hydrocortisone to protect LPS-induced sepsis mice from liver injury[40]. Su et al. (2014) found that vitamin C supplementation helped to improve liver function and play an anti-hepatotoxic role in CCl_4-induced liver injury mice[41]. Glucuronate, a precursor of Vitamin C, is directly formed from UDP-glucuronate in the liver[42]. Several studies have demonstrated that polysaccharides containing glucuronate and other components increase antioxidant enzymes' activity in the serum and liver of mice with alcoholic liver disease while also decreasing inflammatory factors associated with liver injury[43,44]. Glucuronate is converted to L-gulonate by aldehyde reductase, which is then converted to L-gulonolactone by L-gulonolactone synthetase. Finally, L-gulonolactone is oxidized to ascorbate by L-gulonolactone oxidase[45]. In our study, the ascorbate and aldarate metabolism pathways showed significant enrichment with three distinct metabolites: β-D-glucuronoside, glucuronate, and L-gulonate, and treatment with CP and quercetin increased their levels in mouse serum, suggesting that CP and quercetin may promote ascorbate synthesis by up-regulating the levels of β-D-glucuronoside, glucuronate, and L-gulonate, thereby enhancing antioxidant capacity and exerting anti-inflammatory effects in ALI mice. Western blot analysis further confirmed that CP and quercetin have anti-inflammatory and antioxidant effects.

In recent years, the gut microbiota has emerged as an important factor contributing to host health regulation[46]. The liver plays a crucial role in regulating metabolic and immune responses. Excessive inflammation or immune response in the liver can impair pathogen clearance and disrupt hepatic metabolism, thereby exacerbating intestinal barrier dysfunction and disrupting gut microbiota balance. In turn, gut microbiota disorders and heightened intestinal permeability facilitate the overgrowth of pathogenic microorganisms and the translocation to the lymphatic and portal venous systems, thereby impairing the body's defense against infections or injuries and exacerbating hepatic injury[47]. This interaction between the gut microbiota and the liver, is recognized as a promising therapeutic target for treating sepsis-induced liver injury[48]. The present study showed that LPS stimulation caused gut microbiota disruption in mice with ALI, whereas CP and quercetin pretreatment mitigated this disruption, which tended to be consistent with the gut microbiota diversity of the normal group. Probiotics help restore gut microbiota balance and enhance intestinal barrier integrity[49]. Multiple studies have highlighted the important role of probiotics in treating liver injury. *Lactobacillus* supplementation has been shown to effectively reduce the inflammatory response associated with D-galactosamine-induced ALI in rats, ameliorate liver tissue abnormalities, and restore balance to the gut microbiota[50]. *Dubosiella*, a symbiotic beneficial bacterium discovered in recent years, has demonstrated protective efficacy against nonalcoholic

fatty liver disease (NAFLD) in mice[51]. Furthermore, research indicated that the pro-inflammatory bacterium *Alistipes* was notably prevalent in colitis mice[52]. In our study, CP and quercetin pretreatment increased the relative abundance of *Lactobacillus* and *Dubosiella* while reducing *Alistipes* in ALI mice, thereby ameliorating gut microbiota disturbance. Furthermore, the Spearman correlation analysis revealed significant negative correlations between *Dubosiella* and TNF-α, IL-1β, and IL-6, whereas *Alistipes* exhibited significant positive correlations with TNF-α and IL-1β, demonstrating the protective effects of propolis and its active ingredients on ALI.

In conclusion, the integration of network pharmacology, metabolomics, and gut microbiota analysis demonstrated that CP and quercetin effectively reduced pathological injury and inflammation and partially restored the ecology of gut microbiota and metabolic disturbances in LPS-induced ALI mice. Based on previous studies, this study extends the potential role of propolis and its major components in ameliorating inflammation in ALI through a new research perspective, which provides data support for future exploration and development of propolis and its major components.

Materials and methods

Chemicals and reagents

Quercetin (S25567) was procured from Shanghai Yuanye Biotechnology (Shanghai, China) with purity ≥ 97%. LPS (*Escherichia coli* O111:B4) was obtained from Sigma-Aldrich (USA). TRIeasy™ Total RNA Extraction Reagent was obtained from Yeasen Biotechnology (Shanghai, China). PrimeScript™ RT Master Mix reverse transcription kit and TB Green Premix EX Taq™ II were obtained from Takara Bio (Beijing, China). Primer's synthesis was performed by Sangon Biotech (Shanghai, China), and ELISA kits were supplied by MultiSciences Biotechnology Co., Ltd. (Hangzhou, China).

Preparation and analysis of the chinese propolis (CP) ethanol extract

CP was sourced from Changge County, Henan Province, China, in 2023 (voucher specimen no. CP23091002), and poplar (*Populus* spp.) was the main plant source. The extraction method of CP was consistent with one of our previous studies[53]. Through ultra-performance liquid chromatography-tandem mass spectrometry (UPLC-MS/MS), the chemical components of CP were analyzed, and specific conditions agreed with earlier research[54].

Network pharmacological analysis

TCMSP and the ETCM 1.0 database were used to screen active ingredients and collect their relevant targets. The screening criteria for active ingredients in the TCMSP database included oral bioavailability (OB) ≥ 30% and drug-likeness (DL) ≥ 0.18. In addition, in the ETCM database, the screening criteria for "druglikeness grading" was set to "moderate" or "good.". A search for "acute liver injury" was conducted in two databases, Genecard and OMIM. The retrieved targets were normalized to their respective gene names using the Uniprot database. The target genes associated with CP and ALI were then inputted into the Bioinformatics online platform, followed by the generation of Venn diagrams to confirm the common targets. These common targets were then uploaded to the STRING 12.0 database. For the analysis, the species was specified as "*Homo sapiens*," and the "minimum required interaction score" was set to the "highest confidence of 0.9" to generate the PPI network and obtain the TSV format file. The acquired TSV files were imported into Cytoscape 3.7.2 software, employing the "Network Analyzer" tool to compute the degree values. The analyses of Gene Ontology (GO) and Kyoto Encyclopedia of Genes and Genomes (KEGG) were carried out to identify the biological processes (BP), cellular components (CC), molecular functions (MF), and signaling pathways of the active ingredients of CP in the treatment of ALI through the DAVID database. The network of the "CP-key components-common targets-major signaling pathways-ALI" was constructed in Cytoscape 3.7.2 software, employing the "Network Analyzer" tool to compute the degree values and thereby acquire the core ingredients. Table S4 contains the URLs for all databases and online platforms that were used in this study.

Molecular docking

The top three core components of CP were identified as ligands, and their 3D structures were searched from the PubChem database. Among the top 30 hub genes, TNF-α, IL-6, IL-1β, and IFN-γ served as receptors. All receptors were imported to the RCSB PDB database, and the best appropriate crystal structure for the hub gene was chosen while the related PDB file was downloaded. The crystal structure was then treated as follows: water molecules and superfluous ligands were deleted, followed by the addition of hydrogen. Molecular docking was done with the AutoDock Vina 1.1.2 software. The protein pocket coordinates and grid box size are detailed in Table S5. Lastly, the results were visualized using PyMOL 2.4 software.

Animals experiment

Male C57BL/6 J mice (seven-week-old, 22.0 ± 1 g) were procured from Jinan Pengyue Laboratory Animal Breeding Co. Ltd. (Jinan, China; License No. SCXK (LU) 20190003). The mice were housed in an environment with a temperature of 22 ± 2 °C and 55%±15% humidity, under a 12-hour light/dark cycle. All animal experiments followed the Chinese Guidelines for the Care and Use of Laboratory Animals, which were approved by Liaocheng University's Special Committee on Scientific Research Ethics (2023103106).

Five groups ($n = 8$) consisting of the normal group (NOR), model group (LPS), low-dose propolis treated group (CPL, 150 mg/kg), high-dose propolis treated group (CPH, 300 mg/kg), and quercetin treated group (QR, 50 mg/kg) were randomly selected from a total of 40 mice. 0.5% gum tragacanth was used to gavage the normal and model groups, whereas the CP-treated and quercetin-treated groups gavaged propolis and quercetin, respectively. Except for the normal group, all mice received an injection of LPS (15 mg/kg) twenty-four hours

after the final dose, and all mice were euthanized 12 h by cervical dislocation after the tail vein injection. Whole blood, liver, spleen, kidney tissues, and cecal contents were collected.

Histopathological evaluation

Liver tissues were fixed with 4% paraformaldehyde, and then hematoxylin and eosin (H&E) staining was performed after paraffin embedding. An inverted microscope was used to observe the paraffin slices.

Enzyme-linked immunosorbent assay (ELISA)

The pro-inflammatory factors, including TNF-α, IL-1β, and IL-6, in the serum were measured using the ELISA kits following the manufacturer's instructions.

RNA isolation and RT-qPCR

The TRIeasy™ Total RNA Extraction Reagent was used to isolate mouse liver tissue's RNA. Use of the NanoDrop One (Thermo Fisher Scientific, USA) to determine RNA content. For the synthesis of cDNA templates, the reverse transcription kit was used. qPCR was performed in a real-time quantitative PCR system (CFX96, BIO-RAD) using the TB Green Premix EX Taq™ II kit. All primers were synthesized by Sangon Biotech (Table S6). Data were analyzed using the $2^{-\Delta\Delta Ct}$ method, with β-actin serving as the reference gene for normalizing the expression levels of the target gene.

Untargeted metabolomics of serum

A total of 400 µL of a methanol/acetonitrile solvent mixture (1:1, v/v), pre-cooled, was mixed with 100 µL of serum. After vortexing for 30 s and sonication for 10 min in an ice water bath at 4 °C, the mixture was kept overnight at −80 °C. Subsequently, the supernatant was collected after centrifugation at 12,000 rpm and 4 °C for 15 min, followed by drying under low-temperature vacuum conditions. The dried material was then re-solubilized, sonicated for 10 min at 4 °C, and kept overnight at −80 °C. After centrifugation at 12,000 rpm and 4 °C for 15 min, the supernatant was moved to a sample vial for analysis. Mouse serum samples underwent untargeted metabolomics analysis using ultra-high-performance liquid chromatography/quadrupole time-of-flight mass spectrometry system (UHPLC/Q-TOF-MS), and the detailed conditions and data processing were consistent with our previous findings[55].

The Bioinformatics online platform was employed to generate principal components analysis (PCA) score plots, cluster heatmaps, and volcano plots. Orthogonal partial least-squares discrimination analysis (OPLS-DA) modeling was carried out using SIMCA 14.1 software. Serum metabolites were subjected to enrichment analysis for KEGG metabolic pathways using the MetaboAnalyst 6.0 online platform.

DNA extraction and analysis of 16 S rRNA sequencing

Genomic DNA was extracted from cecal contents following the instructions of the E.Z.N.A.® soil DNA kit (Omega Bio-Tek, USA), and the quality of the extracted DNA was detected by 1% agarose gel electrophoresis, and DNA concentration and purity were determined using a NanoDrop 2000 spectrophotometer. The hypervariable region V3-V4 of 16 S rRNA was amplified using primers 338 F (5'-ACTCCTACGGGGAGGCAGCAG-3') and 806R (5'-GGACTACHVGGTWTCTAAT-3') by a PCR instrument. The recovered products were purified with the AxyPrep DNA Gel Extraction Kit (Axygen Biosciences, USA), electrophoresed on 2% agarose gels, and quantified using a Quantus™ Fluorometer (Promega, USA). 16 S rRNA sequencing was performed using Illumina's Miseq PE300/NovaSeq PE250 platform through a standard protocol (Shanghai Majorbio Bio-Pharm Technology Co., Ltd.). Sequences were OTU clustered and annotated for species classification using the RDP classifier (version 2.2).

Using Mothur version 1.30.2 software to analyze the alpha diversity. Beta diversity distance matrices were calculated using QIIME software, and then principal co-ordinates analysis (PCoA), non-metric multidimensional scaling analysis (NMDS), and partial least squares discriminant analysis (PLS-DA) were analyzed and plotted using the R 3.3.1 vegan package. Utilizing linear discriminant analysis effect size (LEfSe, with LDA > 3) to identify distinct bacterial biomarkers that characterize different groups.

Statistical analyses

All experimental data were replicated more than three times and presented as mean ± S.E.M. The data were statistically analyzed using SPSS 27.0.1 and GraphPad Prism 8.0.2. The Kruskal-Wallis (KW) test or one-way ANOVA was performed to identify significant changes, with $P < 0.05$ indicating statistical significance and different superscript letters denoting significant differences. Spearman correlation analysis at the ChiPlot online platform.

Data availability

The data used to support the findings of this study are included within the article.

Received: 31 July 2024; Accepted: 6 May 2025
Published online: 15 May 2025

References

1. Sforcin, J. M. Biological properties and therapeutic applications of propolis. *Phytother Res.* **30** (6), 894–905. https://doi.org/10.1002/ptr.5605 (2016).
2. Vasques, F., Cavazza, A. & Bernal, W. Acute liver failure. *Curr. Opin. Crit. Care.* **28** (2), 198–207. https://doi.org/10.1097/mcc.0000000000000923 (2022).

3. Milosevic, I. et al. Gut-liver axis, gut microbiota, and its modulation in the management of liver diseases: a review of the literature. *Int. J. Mol. Sci.* **20** (2). https://doi.org/10.3390/ijms20020395 (2019).
4. Ahmed, O., Robinson, M. W. & O'Farrelly, C. Inflammatory processes in the liver: divergent roles in homeostasis and pathology. *Cell. Mol. Immunol.* **18** (6), 1375–1386. https://doi.org/10.1038/s41423-021-00639-2 (2021).
5. Yang, Y. M., Kim, S. Y. & Seki, E. Inflammation and liver cancer: molecular mechanisms and therapeutic targets. *Semin Liver Dis.* **39** (1), 26–42. https://doi.org/10.1055/s-0038-1676806 (2019).
6. Tripathi, A. et al. The gut-liver axis and the intersection with the Microbiome. *Nat. Rev. Gastroenterol. Hepatol.* **15** (7), 397–411. https://doi.org/10.1038/s41575-018-0011-z (2018).
7. Zulhendri, F. et al. Recent update on the anti-inflammatory activities of propolis. *Molecules* **27** (23). https://doi.org/10.3390/molecules27238473 (2022).
8. Dos Santos, F. F. et al. A review on the anti-inflammatory activities of Brazilian green, brown and red propolis. *J. Food Biochem.* **46** (10), e14350. https://doi.org/10.1111/jfbc.14350 (2022).
9. Türkez, H., Yousef, M. I. & Geyikoglu, F. Propolis prevents aluminium-induced genetic and hepatic damages in rat liver. *Food Chem. Toxicol.* **48** (10), 2741–2746. https://doi.org/10.1016/j.fct.2010.06.049 (2010).
10. da Silva, S. S. et al. Propolis reduces leishmania amazonensis-induced inflammation in the liver of BALB/c mice. *Parasitol. Res.* **115** (4), 1557–1566. https://doi.org/10.1007/s00436-015-4890-4 (2016).
11. Laaroussi, H. et al. Protective effect of honey and propolis against gentamicin-induced oxidative stress and hepatorenal damages. *Oxid Med Cell Longev.* 9719906. (2021). https://doi.org/10.1155/2021/9719906 (2021).
12. Wu, G., Win, S., Than, T. A., Chen, P. & Kaplowitz, N. Gut microbiota and liver injury (i)-acute liver injury. *Adv. Exp. Med. Biol.* **1238**, 23–37. https://doi.org/10.1007/978-981-15-2385-4_3 (2020).
13. Cai, W. et al. Ethanol extract of propolis prevents high-fat diet-induced insulin resistance and obesity in association with modulation of gut microbiota in mice. *Food Res. Int.* **130**, 108939. https://doi.org/10.1016/j.foodres.2019.108939 (2020).
14. Chien, Y. H., Yu, Y. H. & Chen, Y. W. Taiwanese green propolis ameliorates metabolic syndrome via remodeling of white adipose tissue and modulation of gut microbiota in diet-induced obese mice. *Biomed. Pharmacother.* **160**, 114386. https://doi.org/10.1016/j.biopha.2023.114386 (2023).
15. Okamura, T. et al. Brazilian green propolis improves gut microbiota dysbiosis and protects against sarcopenic obesity. *J. Cachexia Sarcopenia Muscle.* **13** (6), 3028–3047. https://doi.org/10.1002/jcsm.13076 (2022).
16. Son, G., Kremer, M. & Hines, I. N. Contribution of gut bacteria to liver pathobiology. *Gastroenterol. Res. Pract.* https://doi.org/10.1155/2010/453563 (2010). (2010).
17. Ji, Y., Yin, Y., Li, Z. & Zhang, W. Gut microbiota-derived components and metabolites in the progression of non-alcoholic fatty liver disease (NAFLD). *Nutrients* **11** (8). https://doi.org/10.3390/nu11081712 (2019).
18. Zhang, R., Zhu, X., Bai, H. & Ning, K. Network Pharmacology databases for traditional Chinese medicine: review and assessment. *Front. Pharmacol.* **10**, 123. https://doi.org/10.3389/fphar.2019.00123 (2019).
19. Kasote, D., Bankova, V. & Viljoen, A. M. Propolis: chemical diversity and challenges in quality control. *Phytochem Rev.* **21** (6), 1887–1911. https://doi.org/10.1007/s11101-022-09816-1 (2022).
20. Lu, Y. et al. Fuzhengjiedu formula exerts protective effect against LPS-induced acute lung injury via gut-lung axis. *Phytomedicine* **123**, 155190. https://doi.org/10.1016/j.phymed.2023.155190 (2024).
21. Carr, A. C. & Maggini, S. Vitamin C and immune function. *Nutrients* **9** (11). https://doi.org/10.3390/nu9111211 (2017).
22. Rajput, S. A. et al. Luteolin alleviates aflatoxinB(1)-induced apoptosis and oxidative stress in the liver of mice through activation of Nrf2 signaling pathway. *Antioxidants* **10** (8). https://doi.org/10.3390/antiox10081268 (2021).
23. Kemelo, M. K., Pierzynová, A., Kutinová Canová, N., Kučera, T. & Farghali, H. The involvement of Sirtuin 1 and Heme Oxygenase 1 in the hepatoprotective effects of Quercetin against carbon tetrachloride-induced sub-chronic liver toxicity in rats. *Chem. Biol. Interact.* **269**, 1–8. https://doi.org/10.1016/j.cbi.2017.03.014 (2017).
24. Lee, C., Yoon, S. & Moon, J. O. Kaempferol suppresses carbon tetrachloride-induced liver damage in rats via the MAPKs/NF-κB and AMPK/Nrf2 signaling pathways. *Int. J. Mol. Sci.* **24** (8). https://doi.org/10.3390/ijms24086900 (2023).
25. El-Haskoury, R. et al. Antioxidant activity and protective effect of propolis against carbon tetrachloride-induced liver and kidney injury by modulation of oxidative parameters. *Vet. World.* **14** (12), 3076–3083. https://doi.org/10.14202/vetworld.2021.3076-3083 (2021).
26. Jin, Y. et al. Quercetin attenuates toosendanin-induced hepatotoxicity through inducing the Nrf2/GCL/GSH antioxidant signaling pathway. *Acta Pharmacol. Sin.* **40** (1), 75–85. https://doi.org/10.1038/s41401-018-0024-8 (2019).
27. Bailey, S. A., Zidell, R. H. & Perry, R. W. Relationships between organ weight and body/brain weight in the rat: what is the best analytical endpoint? *Toxicol. Pathol.* **32** (4), 448–466. https://doi.org/10.1080/01926230490465874 (2004).
28. Nemethova, V. et al. Therapeutic oligonucleotide ASC1R shows excellent tolerability and remarkable efficacy in reducing SARS-CoV-2 mRNA levels in C57BL/6 mice. *Biomed. Pharmacother.* **180**, 117587. https://doi.org/10.1016/j.biopha.2024.117587 (2024).
29. Li, Q. et al. Irisin alleviates LPS-induced liver injury and inflammation through Inhibition of NLRP3 inflammasome and NF-κB signaling. *J. Recept Signal. Transduct. Res.* **41** (3), 294–303. https://doi.org/10.1080/10799893.2020.1808675 (2021).
30. Xu, L. et al. Hepatic recruitment of eosinophils and their protective function during acute liver injury. *J. Hepatol.* **77** (2), 344–352. https://doi.org/10.1016/j.jhep.2022.02.024 (2022).
31. Bujak, R., Struck-Lewicka, W., Markuszewski, M. J. & Kaliszan, R. Metabolomics for laboratory diagnostics. *J. Pharm. Biomed. Anal.* **113**, 108–120. https://doi.org/10.1016/j.jpba.2014.12.017 (2015).
32. Le, T. T. et al. Disruption of uridine homeostasis links liver pyrimidine metabolism to lipid accumulation. *J. Lipid Res.* **54** (4), 1044–1057. https://doi.org/10.1194/jlr.M034249 (2013).
33. Sun, H. et al. Functional metabolomics discover Pentose and glucuronate interconversion pathways as promising targets for Yang Huang syndrome treatment with Yinchenhao Tang. *RSC Adv.* **8** (64), 36831–36839. https://doi.org/10.1039/c8ra06553e (2018).
34. Giustina, A. D. et al. Vitamin B6 reduces oxidative stress in lungs and liver in experimental sepsis. *Acad. Bras. Cienc.* **91** (4), e20190434. https://doi.org/10.1590/0001-3765201920190434 (2019).
35. Zhou, C. et al. Metabolism of glycerophospholipid, bile acid and retinol is correlated with the early outcomes of autoimmune hepatitis. *Mol. Biosyst.* **12** (5), 1574–1585. https://doi.org/10.1039/c6mb00092d (2016).
36. Guth, I. et al. Caffeine attenuates liver damage and improves neurologic signs in a rat model of hepatic encephalopathy. *Rev. Gastroenterol. Mex (Engl Ed).* **87** (2), 159–169. https://doi.org/10.1016/j.rgmxen.2022.03.004 (2022).
37. Liu, Q. et al. Ginseng polysaccharide components attenuate obesity and liver lipid accumulation by regulating fecal microbiota and hepatic lysine degradation. *Int. J. Biol. Macromol.* **269(Pt 1)**, 131872. https://doi.org/10.1016/j.ijbiomac.2024.131872 (2024).
38. Régnier, M., Polizzi, A., Guillou, H. & Loiseau, N. Sphingolipid metabolism in non-alcoholic fatty liver diseases. *Biochimie* **159**, 9–22. https://doi.org/10.1016/j.biochi.2018.07.021 (2019).
39. Ho, H. L. et al. Ascorbate lacks significant influence in rats with bile duct ligation-induced liver injury. *J. Chin. Med. Assoc.* **80** (9), 539–550. https://doi.org/10.1016/j.jcma.2017.03.010 (2017).
40. Xu, Y. Y. et al. Ascorbic acid and hydrocortisone synergistically inhibit septic organ injury via improving oxidative stress and inhibiting inflammation. *Immunopharmacol. Immunotoxicol.* **44** (5), 786–794. https://doi.org/10.1080/08923973.2022.2082978 (2022).
41. Su, M., Chen, H., Wei, C., Chen, N. & Wu, W. Potential protection of vitamin C against liver-lesioned mice. *Int. Immunopharmacol.* **22** (2), 492–497. https://doi.org/10.1016/j.intimp.2014.07.034 (2014).

42. Linster, C. L. & Van Schaftingen, E. Glucuronate, the precursor of vitamin C, is directly formed from UDP-glucuronate in liver. *Febs J.* **273** (7), 1516–1527. https://doi.org/10.1111/j.1742-4658.2006.05172.x (2006).
43. Jiang, W. et al. Echinacea purpurea polysaccharide prepared by fractional precipitation prevents alcoholic liver injury in mice by protecting the intestinal barrier and regulating liver-related pathways. *Int. J. Biol. Macromol.* **187**, 143–156. https://doi.org/10.1016/j.ijbiomac.2021.07.095 (2021).
44. Wang, K. L. et al. Structural characterization and anti-alcoholic liver injury activity of a polysaccharide from coriolus versicolor mycelia. *Int. J. Biol. Macromol.* **137**, 1102–1111. https://doi.org/10.1016/j.ijbiomac.2019.06.242 (2019).
45. Linster, C. L., Van Schaftingen, E. & Vitamin, C. Biosynthesis, recycling and degradation in mammals. *Febs J.* **274** (1), 1–22. https://doi.org/10.1111/j.1742-4658.2006.05607.x (2007).
46. de Vos, W. M., Tilg, H., Van Hul, M. & Cani, P. D. Gut Microbiome and health: mechanistic insights. *Gut* **71** (5), 1020–1032. https://doi.org/10.1136/gutjnl-2021-326789 (2022).
47. Liang, H. et al. Metformin attenuated sepsis-related liver injury by modulating gut microbiota. *Emerg. Microbes Infect.* **11** (1), 815–828. https://doi.org/10.1080/22221751.2022.2045876 (2022).
48. Sun, J. et al. Gut-liver crosstalk in sepsis-induced liver injury. *Crit. Care*. **24** (1), 614. https:/ (2020).
49. Mijangos-Trejo, A. et al. Prebiotics and probiotics: therapeutic tools for nonalcoholic fatty liver disease. *Int. J. Mol. Sci.* **24** (19). https://doi.org/10.3390/ijms241914918 (2023).
50. Wang, Q. et al. Lactobacillus helveticus R0052 alleviates liver injury by modulating gut Microbiome and metabolome in D-galactosamine-treated rats. *Appl. Microbiol. Biotechnol.* **103** (23–24), 9673–9686. https://doi.org/10.1007/s00253-019-10211-8 (2019).
51. Ye, X. et al. Fgf21-Dubosiella axis mediates the protective effects of exercise against NAFLD development. *Life Sci.* **334**, 122231. https://doi.org/10.1016/j.lfs.2023.122231 (2023).
52. Zou, Y., Ding, W., Wu, Y., Chen, T. & Ruan, Z. Puerarin alleviates inflammation and pathological damage in colitis mice by regulating metabolism and gut microbiota. *Front. Microbiol.* **14**, 1279029. https://doi.org/10.3389/fmicb.2023.1279029 (2023).
53. Liu, H. et al. Bioactive components and mechanisms of Poplar propolis in inhibiting proliferation of human hepatocellular carcinoma HepG2 cells. *Biomed. Pharmacother.* **144**, 112364. https://doi.org/10.1016/j.biopha.2021.112364 (2021).
54. Mei, S., He, Z. & Zhang, J. Identification and analysis of major flavor compounds in radish taproots by widely targeted metabolomics. *Front. Nutr.* **9**, 889407. https://doi.org/10.3389/fnut.2022.889407 (2022).
55. Guo, Y. et al. Integration with transcriptomic and metabolomic analyses reveals the in vitro cytotoxic mechanisms of Chinese Poplar propolis by triggering the glucose metabolism in human hepatocellular carcinoma cells. *Nutrients* **15** (20). https://doi.org/10.3390/nu15204329 (2023).

Acknowledgements
The author acknowledged gratitude to all the staff members involved in the research.

Author contributions
Z.-X.L.: Investigation, Data curation, Formal analysis, and interpretation of data, Model construction. Z.-Z.L. and Y.-Y.G.: Investigation, Data curation, Formal analysis. Y.-J.L. and H.-Z.X.: Project administration, Conceptualization, Methodology, Investigation, Writing review & editing. All authors read and approved the final manuscript.

Funding
This work was supported by a grant from the Shandong Province Modern Agricultural Technology System (SDAIT-24-05), Shandong Provincial Natural Science Foundation of China (ZR2021MC110), and Taishan Scholar Foundation of Shandong Province (NO. tsqn202211172).

Declarations

Competing interests
The authors declare no competing interests.

Ethics approval
All animal experiments followed the Chinese Guidelines for the Care and Use of Laboratory Animals, which were approved by Liaocheng University's Special Committee on Scientific Research Ethics (2023103106), and we confirm the study is reported in accordance with ARRIVE guidelines.

Conflict of interest
The authors declare that there are no conflicts of interest.

Additional information
Supplementary Information The online version contains supplementary material available at https://doi.org/10.1038/s41598-025-01343-1.

Correspondence and requests for materials should be addressed to Y.L. or H.X.